Journal of Biomedical Optics

BiomedicalOptics.SPIEDigitalLibrary.org

Determination of optical properties of human brain tumor tissues from 350 to 1000 nm to investigate the cause of false negatives in fluorescence-guided resection with 5-aminolevulinic acid

Norihiro Honda
Katsunori Ishii
Yoshinaga Kajimoto
Toshihiko Kuroiwa
Kunio Awazu

SPIE.

Norihiro Honda, Katsunori Ishii, Yoshinaga Kajimoto, Toshihiko Kuroiwa, Kunio Awazu, "Determination of optical properties of human brain tumor tissues from 350 to 1000 nm to investigate the cause of false negatives in fluorescence-guided resection with 5-aminolevulinic acid," *J. Biomed. Opt.* **23**(7), 075006 (2018), doi: 10.1117/1.JBO.23.7.075006.

Determination of optical properties of human brain tumor tissues from 350 to 1000 nm to investigate the cause of false negatives in fluorescence-guided resection with 5-aminolevulinic acid

Norihiro Honda,[a,b] Katsunori Ishii,[b] Yoshinaga Kajimoto,[c] Toshihiko Kuroiwa,[c] and Kunio Awazu[b,d,e,*]
[a]Osaka University, Institute for Academic Initiatives, Interdisciplinary Program for Biomedical Sciences, Suita, Osaka, Japan
[b]Osaka University, Graduate School of Engineering, Suita, Osaka, Japan
[c]Osaka Medical College, Department of Neurosurgery, Takatsuki, Osaka, Japan
[d]Osaka University, Graduate School of Frontier Biosciences, Suita, Osaka, Japan
[e]Osaka University, Global Center for Medical Engineering and Informatics, Suita, Osaka, Japan

Abstract. The optical properties of human brain tumor tissues, including glioblastoma, meningioma, oligodendroglioma, and metastasis, that were classified into "strong," "vague," and "unobservable" fluorescence by a neurosurgeon were measured and compared. The optical properties of the tissues were measured with a double integrating sphere and the inverse Monte Carlo technique from 350 to 1000 nm. Using reasons of *ex-vivo* measurement, the optical properties at around 420 nm were potentially affected by the hemoglobin content in tissues. Significant differences were not observed between the optical properties of the glioblastoma regions with "strong" and "unobservable" fluorescence. Sections of human brain tumor tissue with "strong" and "unobservable" fluorescence were stained with hematoxylin and eosin. The cell densities [mean ± standard deviation (S.D.)] in regions with "strong" and "unobservable" fluorescence were $31 \pm 9 \times 10^2$ per mm^2 and $12 \pm 4 \times 10^2$ per mm^2, respectively, which is a statistically significant difference. The higher fluorescence intensity is associated with higher cell density. The difference in cell density modified the scattering coefficient yet it does not lead to significant differences in the reduced scattering coefficient and thus does not affect the propagation of the diffuse fluorescent light. Hence, the false negatives, which mean a brain tumor only shows "unobservable" fluorescence and is hence classified incorrectly as nontumor, in using 5-ALA for detection of human glioblastoma do not result from the differences in optical properties of human brain glioblastoma tissues. Our results suggest that the primary cause of false negatives may be a lack of PpIX or a low accumulation of PpIX. [DOI: 10.1117/1.JBO.23.7.075006]

Keywords: optical properties; malignant brain tumor; 5-aminolevulinic acid; false negative; double integrating sphere; inverse Monte Carlo method.

Paper 170792RRR received Dec. 9, 2017; accepted for publication Jun. 22, 2018; published online Jul. 13, 2018.

1 Introduction

In 1998, the fluorescence-guided resection of malignant gliomas using 5-aminolevulinic acid (5-ALA) was reported by Stummer et al. in Germany.[1] In 2006, Stummer et al. reported that fluorescence-guided resection using 5-ALA not only led to an increase in the complete resection rate but also improved progression-free survival.[2] In addition, the median overall from the time of surgery in patients without residual tumors as a result of complete resection achieved by fluorescence-guided resection with 5-ALA was longer than those in patients with residual contrast-enhancing tumor material.[3] It was reported that even small volumes of residual tumor [radiation therapy oncology group recursive partitioning analysis (RTOG-RPA) classes III–V based on age] was associated with a worse prognosis compared with there being no visible and residual contrast-enhancing tumor.[4] Differences in survival depending on resection status, especially in RPA classes IV and V, support a causal influence of resection on survival. However, fluorescence diagnosis with 5-ALA is very cost effective, whereas there have been problems with false negatives in fluorescence diagnosis; a false negative means that a brain tumor has "unobservable" fluorescence and is hence classified incorrectly as a nontumor.[1]

Fluorescence intensity from PpIX observed through the surgical microscope has been graded according to intensity in two or three stages.[5] On irradiation of violet–blue light to a brain tumor that included PpIX, necrotic tumors usually displayed no or only inhomogeneous red fluorescence. In addition, joining, perfused, and viable tumor tissue was distinguished by its deep red fluorescence, which we call "strong" in this report, whereas normal brain tissue was colored blue. Usually, a transition zone with clearly discernible, but lighter, pink fluorescence was encountered between solidly fluorescing tumor

*Address all correspondence to: Kunio Awazu, E-mail: awazu@see.eng.osaka-u.ac.jp

1083-3668/2018/$25.00

and nonfluorescing blue brain tissue.[5] We term this fluorescence impression "vague." "Strong" fluorescence from the region indicates that the region is highly likely to be tumor. In a primary malignant glioblastoma, the tumor probability (positive predictive value) for tumor tissue that shows strong fluorescence is 100%.[1] Moreover, in the detection of primary malignant glioma tissue using 5-ALA, sensitivity and specificity were 85% and 100%, respectively.[1] However, while diagnosis with 5-ALA by fluorescence provided an excellent ability to predict the presence of abnormal and tumor tissue, the mechanism of selective accumulation of PpIX in tumor tissue has not yet been understood. Pathological findings have revealed that strong correlation exists between tumor aggressiveness and corresponding intraoperative fluorescence.[6] A previous study has indicated that solidly proliferating, central, viable tumors with vascular proliferation are associated with intense red fluorescence, and surrounding infiltrating tumor with moderate to high cell density is associated with pink fluorescence.[5] Histologically, solidly fluorescing tissue generally consisted of coalescent tumor cells, whereas vaguely fluorescing tissue usually represented an infiltrating tumor of intermediate or low cellular density.[5] Their analysis of tumor biopsy specimens revealed infiltrating tumor also to be present beyond vaguely fluorescing tissue portions. Takahashi et al. reported that the high mRNA level of CPOX expression was significantly correlated with the phenotype of strong 5-ALA-induced fluorescence.[7] Elucidation of the cause of false negatives may ameliorate the sensitivity in fluorescence-guided resection for glioblastoma with 5-ALA.

To the best of our knowledge, no reports exist concerning whether the optical properties of false-negative brain tumor tissue differ from those of brain tumor tissue with strong fluorescence, when measured with a double integrating sphere and inverse Monte Carlo methods. If the cell density in the tumor tissue that contains the PpIX increases, the fluorescence intensity of the tumor tissue increases. The purpose of this study is to investigate the effect of optical properties of human brain tumor tissues on the fluorescence intensity. In addition, the cell density of the resected tumor tissue and the tissue that was classified by a neurosurgeon according to observable fluorescence are compared.

2 Materials and Methods

2.1 *Sample*

The specimens were tumor and normal human brain tissues obtained from brain tumor patients undergoing fluorescence-guided resection with 5-ALA at the Department of Neurosurgery, Osaka Medical College. A study protocol approved by the Institutional Review Board of Osaka Medical College was followed and a consent form was signed by each participating patient before the surgery.

2.1.1 *Samples for optical property measurements*

Fresh samples were delivered within 1 to 2 h after their acquisition from the operation room. Measurements of diffuse reflectance and total transmittance were conducted within 3 to 12 h after resection. Samples were stored at low temperature (1°C to 4°C) in saline solution until sample preparation for spectroscopic measurement. A total of 32 samples of human brain tumor tissues that were classified by histological type by a pathologist were investigated: glioblastoma ($n = 14$), meningioma ($n = 9$), oligodendroglioma ($n = 3$), and metastasis ($n = 6$). These tumor tissues were classified into three groups according to their fluorescence, "strong" ($n = 15$), "vague" ($n = 6$), and "unobservable" ($n = 11$) by a neurosurgeon. (Fluorescence intensity was also measured using a spectral radiance measuring system. The excitation light from a 405-nm LED was irradiated to samples at an irradiance of 10 mW/cm^2. The measurement distance was 70 mm and the diameter of the spot size on the sample was 3 mm.[8]) In addition, four samples of normal human brain tissue [white matter ($n = 2$) and gray matter ($n = 2$)] were investigated. The materials were stored at low temperature in saline solution until spectroscopic investigation. The sample size is the number of individuals.

2.1.2 *Samples for histological evaluation*

Eleven samples of tumor tissues [unclassified glioma "strong" ($n = 5$), unclassified glioma "unobservable" ($n = 3$), meningioma "strong" ($n = 2$), and metastasis "strong" ($n = 1$)] were used. These tumor tissues were classified into three groups according to their fluorescence, "strong" ($n = 8$) and "unobservable" ($n = 3$) by a neurosurgeon. The cell density was evaluated from pathological specimens. The data of cell density are used purely as ancillary data. The number of samples differs between Secs. 2.1.1 and 2.1.2.

2.2 *Sample Preparation for Optical Properties Measurements*

Sections for spectroscopic measurement were cut into 0.5- or 1-mm-thick slices using surgical knives and scissors, and positioned between slide glasses. The thickness of the samples was controlled using a spacer.

2.3 *Integrating-Sphere Measurements of Diffuse Reflectance and Transmittance*

Optical parameter measurements were performed using a double integrating sphere system as described previously.[9] Samples in glass slides were placed between both spheres, which were 100 mm in diameter. The sample port diameter was chosen as 5 or 10 mm according to the sample size. The diameter of the sample was slightly larger than the sample port. A xenon lamp [L2274(GS) and C8849, Hamamatsu Photonics K.K.] used as the light source. The beam size at the sample was around 1 mm in diameter. For diffuse reflectance and transmittance measurements, an integrating sphere (CSTM-3P-GPS-033SL, Labsphere) was used. The reflected (R_d) and transmitted (T_t) light was detected by a spectrometer (MAYP10161, Maya2000-Pro, Ocean Optics) with an order-sorting and blocking filter and stored in a computer. All samples were measured in the wavelength range from 350 to 1000 nm. Diffuse reflectance and total transmittance were measured at a minimum of five spots in the sample and averaged.

2.4 *Evaluation of Optical Properties of Tissues*

The optical properties from the measured data were calculated using an inverse Monte Carlo technique as described previously.[9] The algorithm consisted of the following steps: (a) estimate a set of optical properties, (b) calculate the reflectance and transmittance with the Monte Carlo code developed by Wang et al.,[10] (c) compare the calculated results with the

measured values of the R_d and T_t, and (d) reiterate the above steps until the calculated and measured values agree within the specified acceptance margin of 99.5%. This iterative process yields the set of optical properties that most closely match the measured values of reflectance and transmittance of the tissue. The crosstalk between the spheres was not taken into account. In these calculations, the anisotropy factor was fixed at 0.9 because this is the typical value in many tissues.[11] Additionally, because the average refractive index of a single cell is 1.38 at 405 nm (as shown in Ref. 12), the refractive index was fixed at 1.38. When considering a photon and several scattering events, the reduced scattering coefficient (μ_s') can be defined[13] to describe a multiple scattering process as $\mu_s' = \mu_s\ (1 - g)$.

2.5 *Histological Analysis*

Sections prepared for histological investigation were stained with hematoxylin and eosin (H&E).

2.6 *Statistical Analysis*

The data are presented as the mean with the standard deviation. Statistical analyses were performed using the Student's t-test with a significance level of $P < 0.05$.

2.7 *Geometry of the Modeled Tissue for Florescence Monte Carlo Simulations*

Homogeneous turbid media including fluorescence was assumed. The model of the tissue was divided into 400 elements in the radial direction, each element being 0.005-cm wide. The z-direction was divided into 200 elements, each element being 0.005-cm long. A pencil beam was assumed to enter the phantom at the point $(r, z) = (0,0)$.

2.8 *Fluorescence Monte Carlo Simulations*

The Monte Carlo technique was employed to yield a probability distribution of the generated fluorescence inside the volume and an intensity at the surface. The fluorescence Monte Carlo simulation developed by Jacques[14] was used. The wavelength of excitation and emission was 405 and 635 nm, respectively. Additional inputs to the Monte Carlo simulations, apart from the optical properties of the different layers and geometry, were the quantum yield, molar extinction constant, and concentration of the fluorescence in the tissue. The glioblastoma of human brain tumor tissues classified as "strong," "vague," and "unobservable" was assumed as the tissue model in simulation. The optical properties used were measured values in this study. The numbers of photons used in each simulation for excitation light and fluorescence emission were 4 and 16 million, respectively. In the simulation, the fluorescence quantum yields of PpIX[15] and PpIX concentration[16] were assumed as 0.011 and 5.8 μmol/L, respectively.

2.9 *Refractive Index and Anisotropy Factor*

The refractive index (n) and anisotropy factor (g) of the tissue model were altered slightly to evaluate their effect on μ_a and μ_s'. Three different simulations were performed, changing the n and g at all wavelengths to 1.40 and 0.95, respectively. In all other aspects, the calculation processes were identical to those described in Sec. 2.4.

3 Results

3.1 *Optical Properties of Human Brain Tumor Tissues with "Strong," "Vague," and "Unobservable" Fluorescence, and Normal Human Brain Tissues*

The absorption coefficient (μ_a) spectra of the human brain tumor tissue from 350 to 1000 nm are shown in Fig. 1(a). There was no significant difference between the μ_a values of brain tumor tissues in regions with "strong," "vague," and "unobservable" fluorescence, as shown in Fig. 1(a). The μ_s' spectra of the brain tumor tissues from 350 to 1000 nm are shown in Fig. 1(c). Again, no statistical difference was

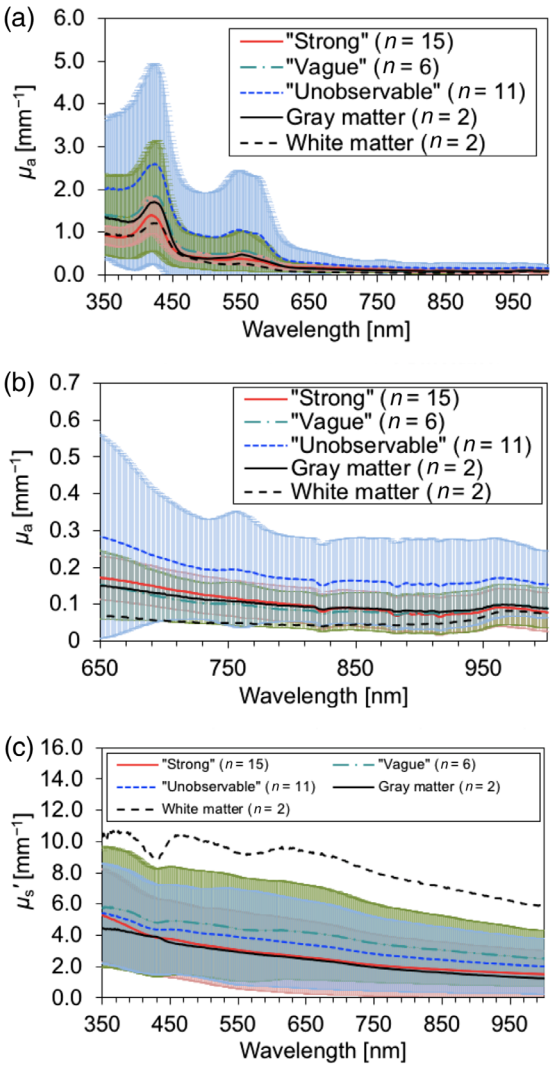

Fig. 1 Optical properties of human brain tumor tissues obtained from glioblastoma, metastasis, meningioma, and oligodendroglioma (classified into three classes according to their fluorescence), normal brain gray matter ($n = 2$), and white matter ($n = 2$). (a) Absorption coefficient μ_a spectra, (b) μ_a spectra magnified scale between 650 and 1000 nm, and (c) reduced scattering coefficient μ_s' spectra.

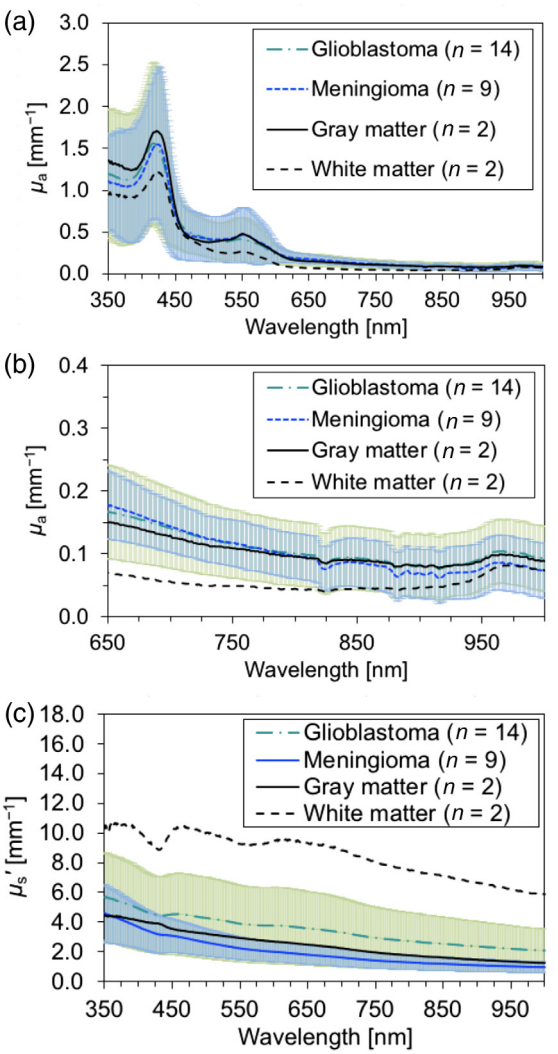

Fig. 2 Optical properties of human glioblastoma ($n = 14$), meningioma ($n = 9$), normal brain gray matter ($n = 2$), and white matter ($n = 2$). (a) Absorption coefficient μ_a spectra, (b) μ_a spectra magnified scale between 650 and 1000 nm, and (c) reduced scattering coefficient μ_s' spectra.

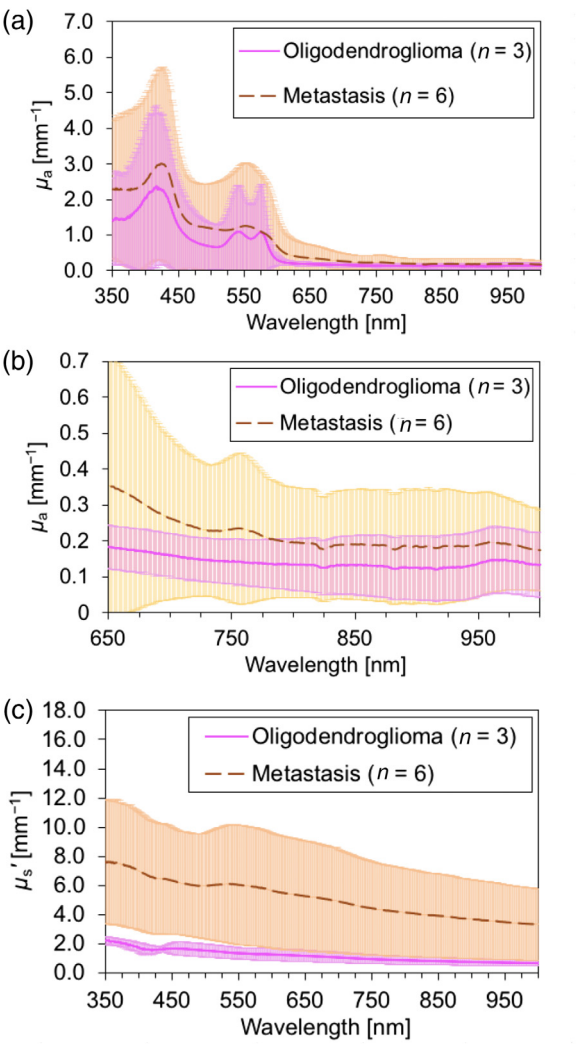

Fig. 3 Optical properties of human oligodendroglioma ($n = 3$) and metastasis ($n = 6$). (a) Absorption coefficient μ_a spectra, (b) μ_a spectra magnified scale between 650 and 1000 nm, and (c) reduced scattering coefficient μ_s' spectra.

observed in the μ_s' of the tumor tissues with "strong," "vague," and "unobservable" fluorescence.

3.2 *Optical Properties of Human Brain Tumor Tissues Classified by Histological Types, and Human Brain Normal Tissues*

There was no significant difference between the μ_a values of tissue with different tumor types (Figs. 2 and 3). The μ_s' values of human brain tumor tissues are shown in Figs. 2 and 3, respectively. The μ_s' values of the glioblastoma tissue were significantly higher than those of the meningioma tissue from 508 to 1000 nm. The μ_s' values of glioblastoma tissue were significantly higher than those of oligodendroglioma tissue at some wavelengths. There was no significant difference between the μ_s' values of glioblastoma and metastasis tissues. The μ_s' values of meningioma tissue at some wavelengths were significantly higher than those of oligodendroglioma tissue. Furthermore, there was no significant difference between the μ_s' values of meningioma and metastasis tissues.

3.3 *Optical Properties of Human Brain Tumor Tissues Classified Following to Histological Types and Fluorescence Intensities*

The optical properties of glioblastoma and meningioma tissues classified according to their fluorescence are shown in Figs. 4 and 5, respectively. There were no significant differences between the μ_a values of glioblastoma tissue region with "strong" and "unobservable" fluorescence in Figs. 4(a) and 4(b). The maximum μ_a values in the absorption band of hemoglobin appeared at 416 and 544 nm in glioblastoma tissue region with "strong" fluorescence. The maximum μ_a values in the absorption band of hemoglobin appeared at 423 and 551 nm in glioblastoma tissue at the region with "unobservable" fluorescence. There were no significant differences between the μ_s' values of glioblastoma tissue in the regions with "strong" and "unobservable" fluorescence in Fig. 4(c). The maximum μ_a values in the absorption band of hemoglobin appeared at 423 and 551 nm in meningioma tissue at the regions with "strong" fluorescence [Fig. 5(a)]. The dips observed for μ_s' in

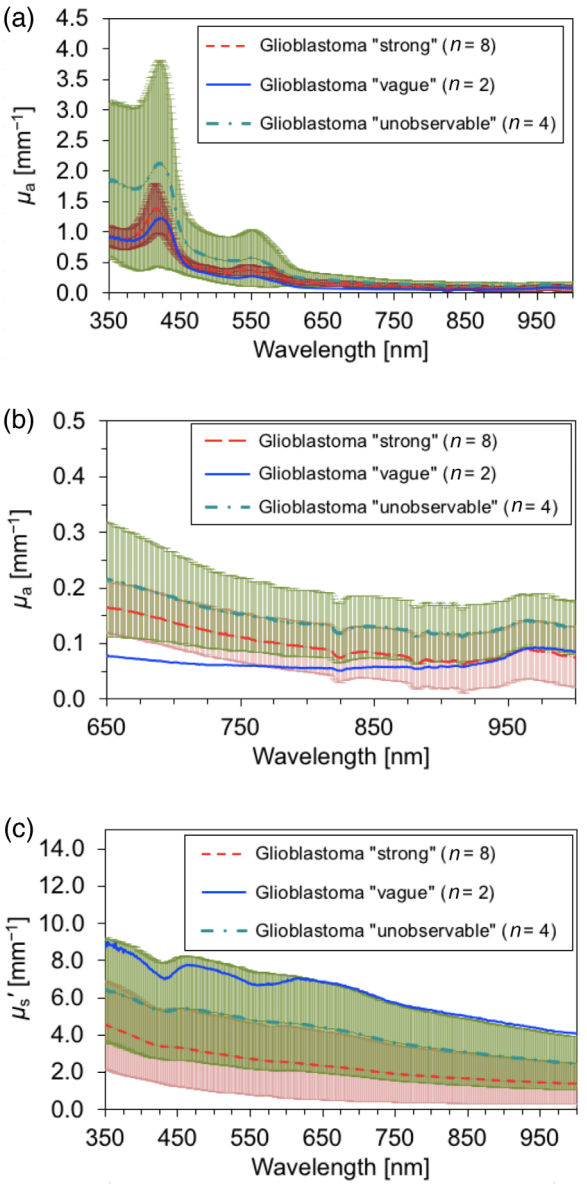

Fig. 4 Optical properties of human glioblastoma [classified into three classes according to their fluorescence: strong ($n = 8$), vague ($n = 2$), and unobservable ($n = 4$)]. (a) Absorption coefficient μ_a, (b) μ_a spectra magnified scale between 650 and 1000 nm, and (c) reduced scattering coefficient μ_s' spectra.

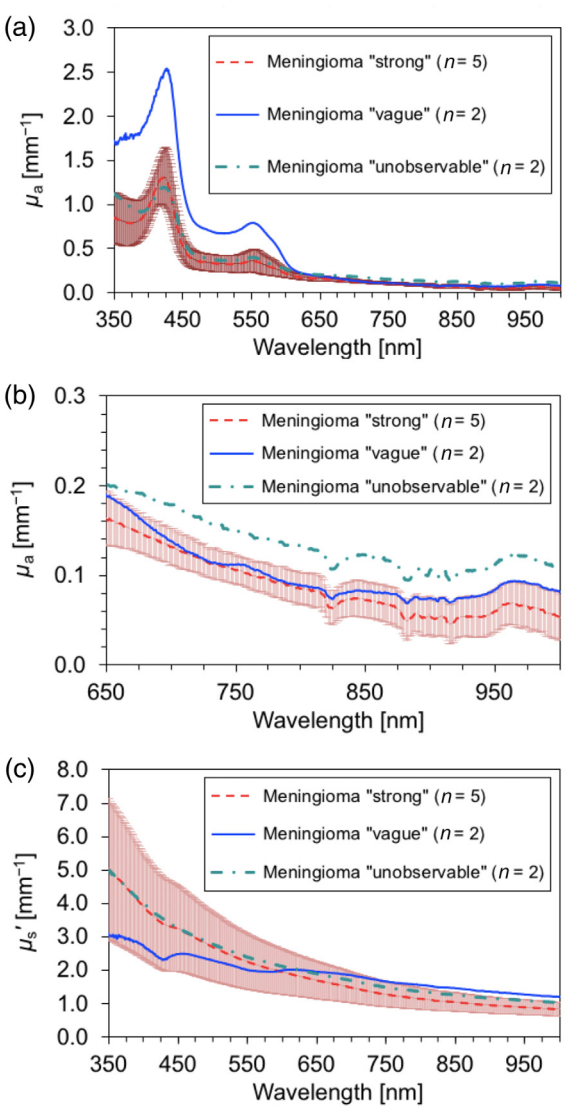

Fig. 5 Optical properties of human meningioma [classified into three classes according to their fluorescence: strong ($n = 5$), vague ($n = 2$), and unobservable ($n = 2$)]. (a) Absorption coefficient μ_a spectra, (b) μ_a spectra magnified scale between 650 and 1000 nm, and (c) reduced scattering coefficient μ_s' spectra.

Figs. 1–5 at 420 nm are probably due to artifacts resulting from the hemoglobin absorption.

3.4 *Correlation Between Visible Fluorescence and Histology*

The sections of human brain tumor tissue, classified as meningioma, metastasis, and unclassified glioma with "strong" and "unobservable" fluorescence were stained with H&E, and histological images are shown in Fig. 6, from which the cell density was estimated. The cell densities [mean ± standard deviation (S.D.)] in regions with "strong" and "unobservable" fluorescence were $31 \pm 9 \times 10^2$ per mm^2 and $12 \pm 4 \times 10^2$ per mm^2, respectively. Thus, there is a statistically significant difference in the cell densities between the regions with "strong" and "unobservable" fluorescence. Meningioma showed typical whorl formation [Fig. 6(c)]. Some nuclei contained clear holes. Spindle-shaped tumor cells with elongated nuclei, forming parallel or storiform bundles, were observed.

3.5 *Correlation Between Visible Fluorescence and the Optical Property of Tissue*

To investigate whether optical properties affect emissions from glioblastoma tissues, the emission was calculated using Monte Carlo simulation (Fig. 7). The maximum fluorescence strength at the surface and the ratio of relative intensity at the surface are shown in Table 1. Although the probability distributions of emitted fluorescence in the three models were different, the intensities at the surface were almost identical.

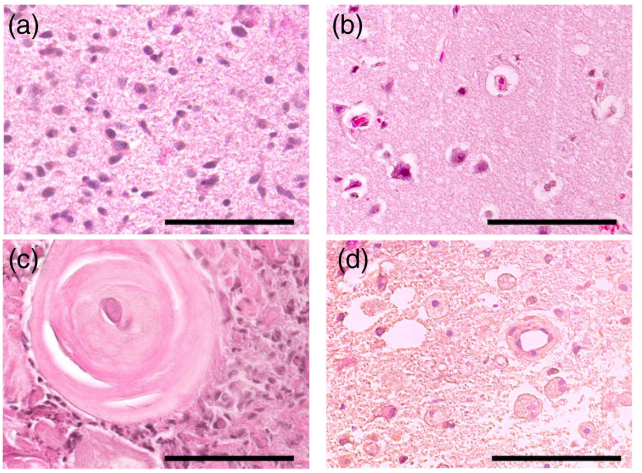

Fig. 6 H&E staining of a tumor section. (a) Regions with "strong" fluorescence and (b) regions with "unobservable" fluorescence in unclassified glioma. (c) Regions of meningioma with "strong" fluorescence and (d) regions of metastasis with "strong" fluorescence. Scale bar, 100 μm.

3.6 *Sensitivity of the Optical Properties to Variations of Reflective Index and Anisotropy Factor*

In Fig. 8(a), the absorption coefficient and the reduced scattering coefficient spectra are presented for different refractive indices. Figure 8(b) shows the absorption coefficient and the reduced scattering coefficient spectra when the anisotropy factor is changed. The absorption coefficient and the reduced scattering coefficient were not changed significantly by changing the refractive index and anisotropy factor.

4 Discussion

The μ_a values of glioblastoma tissue in the region with "strong" fluorescence and "unobservable" fluorescence were compared at 405 and 635 nm, and there was no significant difference as can be seen in Fig. 4(a). Our results have been compared with ones reported by other groups (Table 2).[17–19] The μ_s' values determined by Gebhart et al.[19] are about 1.5 times lower than the values obtained in the present work. However, in that study, the tissues were stored at 193 K until *in-vitro* measurement of the optical properties. Roggan et al.[20] stated that the μ_s of liver tissues is lowered by shock-freezing at 77 K by −21.7% in comparison with the untreated ones. Therefore, this might explain why the μ_s' values estimated in this study are higher than the values reported by Gebhart et al.[19] Pitzschke et al.[21] reported that tissue freezing reduces the μ_s'.

It is difficult to estimate accurately the experimental error in a study of this type in which many independent measurements are conducted. Experimental contributions to the error included the inaccuracy of the spectrometer, which we estimated to be <1% of the full-scale value. This error becomes more prominent as the measured values of R_d and T_t become smaller, such as in

Table 1 Comparison of the maximum emission intensity at the surface of tissues estimated using fluorescence Monte Carlo simulation. The ratio of relative emission intensity is estimated by normalization with the value of the sample classified as "vague." The ratio of emission to excitation at the tissue surface was estimated. In addition, the $1/(\mu_1+\mu_2)$ of tissues with strong and unobservable fluorescence was compared.

		Strong	Vague	Unobservable	*P*-value
Maximum emission intensity	[1/cm^2]	0.16	0.21	0.16	—
Ratio of relative emission intensity	[—]	0.78	1.00	0.77	—
J_em/J_ex	[×10^{-4}]	8.62	4.72	5.92	—
$1/(\mu_1+\mu_2)$		0.21 ± 0.06		0.18 ± 0.08	0.18

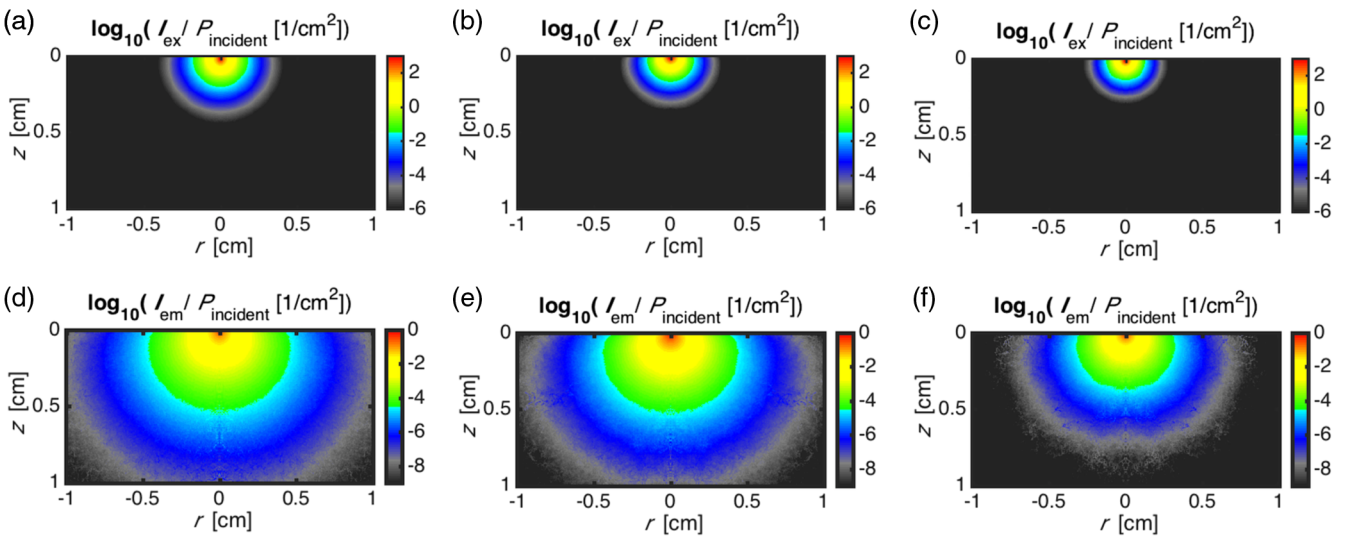

Fig. 7 Upper row: (a) left, the distribution of the excitation light in the "strong" fluorescence human brain tumor model; (b) middle, in the "vague" fluorescence human brain tumor model; and (c) right, in the "unobservable" fluorescence human brain tumor model. Lower row: (d)–(f), corresponding images for the fluorescence emission light at 635 nm.

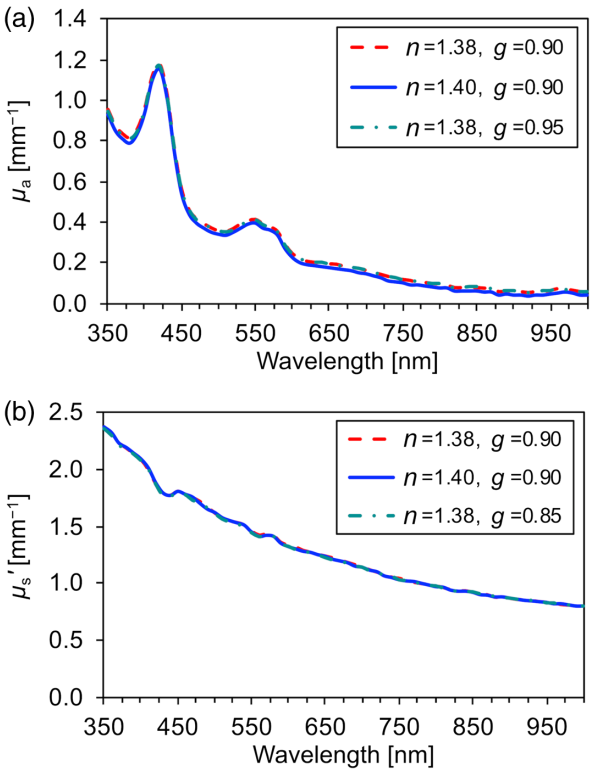

Fig. 8 (a) Absorption coefficient spectra and (b) reduced scattering coefficient spectra of tumor tissue, when the refractive index or the anisotropy factor was changed.

the wavelength range between 350 and 600 nm. Furthermore, there is a significant biological variability between the samples. For example, if the blood of the samples varied, this would be particularly noticeable between 350 and 600 nm. This may have introduced an error in the μ_s' spectra.

Tumors are associated with regions of hypoxia. Solid tumors contain regions at very low oxygen concentrations (hypoxia), often surrounding areas of necrosis.[22] Perhaps, tumor tissues at very low oxygen concentration is account for certain curves in μ_a, mimicking the absorption curve of deoxyhemoglobin, whereas other curves correspond to the oxyhemoglobin form.

The higher fluorescence intensity is associated with higher cell density. However, while a higher cell density was found in "strong" than in "unobservable" fluorescence tissues, this is not reflected in the μ_a and the μ_s' spectra. Perhaps this is caused by the higher μ_a of blood than that of PpIX included in mitochondria; thus the μ_a of blood is prominent in the μ_a of the brain tumor tissue. In addition, the μ_s' is not linearly related with the concentration of scattering molecules for more strongly scattering materials, such as brain tissue. This leads to there being no difference between the μ_s's of "strong" and "unobservable" brain tumor tissue. Thus, the difference of cell density modified the scattering coefficient yet it does not lead to significant differences in the μ_s' and thus does not affect the propagation of the diffuse fluorescent light.

Diaz et al.[23] investigated whether fluorescein had the ability to specifically stain glioma cells in a study of fluorescein uptake by intracranial U87 malignant glioma xenografts in male non-obese diabetic/severe combined immunodeficient mice. In that report, false negatives could be caused by lack of fluorescence in areas of diffuse, low-density cellular infiltration. The results of our study are in agreement with this, as shown in Sec. 3.4. In addition, Bogaards et al.[24] reported that in the majority of animals, complete tumor resection was not achieved owing to small tumor cell nests in the surgical cavity, which were undetectable by fluorescence of PpIX. These could be considered as false negatives for the particular device, 5-ALA dose, and administration time. Moreover, in cases where the tumor invaded beyond the surgical cavity, this would not be detectable by fluorescence imaging of the cavity with fluorescent dye as the effective tissue sampling depth of the blue-light excitation below the exposed tissue surface is <0.5 mm.[25] These reports suggest the lack of fluorescent dye and/or the decline of the excitation energy in the tumor tissue may have the potential to cause false negatives in fluorescence-guided resection. The optical penetration depth (δ) is one of the indices of light attenuation in biological tissue. Thus, the δ values of human brain tumor tissues were calculated from the optical properties shown in Figs. 1–5 and compared. Two equations were used to calculate the optical penetration depth (δ). When $\mu_a \ll 3\ \mu_s'$, the δ can be estimated as[26]

$$\delta = \frac{1}{\sqrt{3\mu_a(\mu_a + \mu_s')}}. \tag{1}$$

When μ_a is comparable with μ_s' ($10\ \mu_a \geq 3\ \mu_s'$), δ was estimated as[27]

$$\delta = \frac{1}{\sqrt{\mu_a(\mu_a + 3\ \mu_s')}}. \tag{2}$$

The δ depends on the wavelength, as shown in Figs. 9–11. The δs at 635 nm in brain tumor tissues at the regions with "strong," "vague," and "unobservable" fluorescence were about 0.98, 0.97, and 0.78 mm, respectively, as shown in Fig. 9. Moreover, to confirm whether there is a difference in δ in glioblastoma tissues between the regions with "strong" and "unobservable" fluorescence, the δ values of glioblastoma tissues were compared [Fig. 11(a)]. The δs at 405 nm in glioblastoma tissues with "strong" and "unobservable" fluorescence were about 0.28 ± 0.08 mm and 0.20 ± 0.05 mm, respectively, and thus are comparable within the error limits. Assuming the attenuation coefficient to be $\mu_1 = 1/\delta_1$ at 405 nm and $\mu_2 = 1/\delta_2$ at 635 nm, the detected fluorescence intensity under a uniform distribution of PpIX of density [PpIX] under pencil illumination is proportional to: $[\mathrm{PpIX}]/(\mu_1 + \mu_2)$. "$1/(\mu_1 + \mu_2)$" and p-values comparing "strong" and "unobservable" fluorescence tissue are shown in Table 1. They were comparable within the error limits. From the result of the fluorescence Monte Carlo simulation (Fig. 7), the ratio of the relative intensity of emission at the surface was almost identical (Table 1). The measured approximate fluorescence intensity ratio of "strong," "vague," and "unobservable" was 2.51:0.49:0.1 by spectroscopy;[8] this explains that this difference is caused by the difference of the concentration of fluorescence, or PpIX.

If *in-vivo* measurement shows that tissue has higher μ_a than in this *ex-vivo* study, the δ would become lower and the detectable fluorescence would be mainly from PpIX included in the tissue in the submillimeter range from the surface. Thus, the effect of optical properties on the false negatives would become smaller or zero as μ_a increases.

In many cases, optical properties change the wavelength-dependent manner and the corresponding excitation and emission intensity changes. However, this situation is restricted to when δ

Table 2 Comparison of (a) mean absorption coefficients, (b) mean reduced scattering coefficients, and (c) optical penetration depths of meningioma and brain tumor. Differences to the means of two measurements are calculated.

	Meningioma			Brain tumor			
Wavelength [nm]	This work	Reference	Difference	This work	Reference	Difference	Ref.
(a)							
630	0.19	0.035	0.16				18
630				0.21	0.081 (glioma)	0.13	19
670	0.16	0.03	0.13				18
670				0.19	0.071 (glioma)	0.12	19
850	0.09	0.025	0.07				18
850				0.11	0.064 (glioma)	0.05	19
(b)							
630	1.88	0.93	0.95				18
630				3.49	2.2 (glioma)	1.3	19
670	1.73	0.9	0.83				18
670				3.31	2.1 (glioma)	1.2	19
850	1.19	0.65	0.54				18
850				2.43	1.8 (glioma)	0.6	19
(c)							
488				0.48	1.4 – 0.5	−0.9 – (−0.02)	17
514				0.52	1.4 – 0.5	−0.9 – 0.02	17
630	1.00	3.1	−2.1				18
630				0.89	1.3 (glioma)	−0.4	19
635				0.91	2.6 – 1.7	−1.7 – (−0.8)	17
670	1.13	3.5	−2.4				18
670				0.99	1.5 (glioma)	−0.5	19
850	2.00	4.4	−2.4				18
850				1.65	1.7 (glioma)	−0.05	19

Note: Svaasand et al.,[17] Yaroslavsky et al.,[18] and Gebhart et al.[19]

is high, or incident light can easily penetrate tissues and the intensity of excitation light becomes high and results in the emission light becoming easy to detect. In 2017, Wirth et al.[28] reported that the depth of fluorescence was estimated under a bulk phantom, having μ_s' of 1.0 mm^{-1} and μ_a of 0.001 mm^{-1}. Although the results by Wirth et al. suggest that the depth of fluorescence was correctly estimated for shallower inclusions, the error of the predicted depth drastically increased for inclusions at depths greater than δ, even when using a correction based on optical properties. With regard to the optical properties of the human glioblastoma tissues, the δ was 0.2 or 0.3 mm at 405 nm. Whether we can recognize, or detect, the PpIX fluorescence emitted from the glioblastoma tissue does not mainly depend on the optical properties but is more strongly affected by the quantity of PpIX present within 0.2- to 0.3-mm depth, or the δ, from the surface when PpIX is excited by the light at 405 nm. Hence, the small amount of PpIX that is contained in the tissue within the depth of optical penetration more strongly affects the false negatives under the conditions that the tissue has low δ.

Technical advances[29–31] have increased the sensitivity of tumor tissue detection using 5-ALA-PpIX, but so far, the sensitivity has not reached 100%.[32,33] The correction of optical properties for the detection of PpIX validated with a phantom was found to be suitable for quantitative fluorescence spectroscopy and imaging.[28,34] If there is a region with high δ in brain

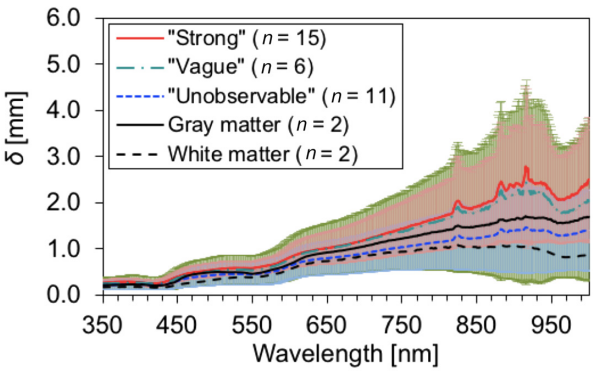

Fig. 9 Optical penetration depths δ of human brain tumor tissues obtained from glioblastoma, metastasis, meningioma, and oligodendroglioma (classified into three classes according to their fluorescence), normal brain gray matter ($n = 2$), and white matter ($n = 2$).

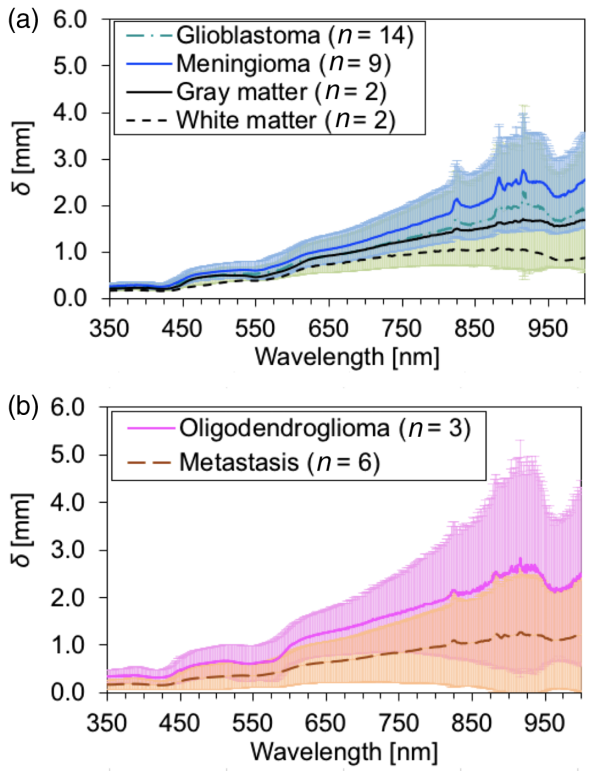

Fig. 10 Optical penetration depth δ spectra of human glioblastoma ($n = 14$), meningioma ($n = 9$), oligodendroglioma ($n = 3$), metastasis ($n = 6$), normal brain gray matter ($n = 2$), and white matter ($n = 2$).

tumor tissue caused by local variation, the method of correction using the optical properties would work effectively in quantitative fluorescence spectroscopy and imaging. *In vivo* measurement of PpIX content in false-negative tissue, such as reported by Valdés et al.,[35] it is also important to reveal the correlation in each patient between the presence of tumor tissue and the corresponding local *in-vivo* optical properties.

Stummer et al.[36] reported that "strong" visual fluorescence in individual samples was related to high cell densities and strong fluorescence, whereas samples designated as "weak" by study surgeons had low cell densities and low spectrometric fluorescence. The mRNA level of ABC transporter ABCG2 was lower

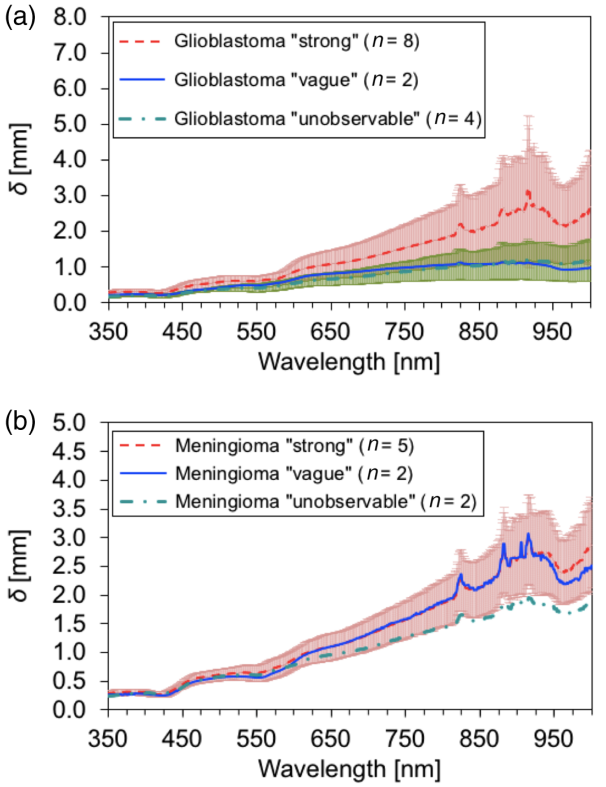

Fig. 11 Optical penetration depth δ spectra of (a) human glioblastoma [classified into three classes according to their fluorescence: strong ($n = 8$), vague ($n = 2$), and unobservable ($n = 4$)], and (b) human meningioma [classified into three classes according to their fluorescence: strong ($n = 5$), vague ($n = 2$), and unobservable ($n = 2$)].

in malignant glioma cells in the brain tumor that exhibited strong fluorescence of PpIX after 5-ALA treatment, whereas the surrounding cells emitted "vague" fluorescence.[37] ABCG2, a porphyrin efflux pump, is downregulated in tumors. These reports and our results suggest that the primary cause of false negatives may be a lack of PpIX or a low accumulation of PpIX in malignant glioblastoma.

5 Conclusion

In human glioblastoma tissue obtained from fluorescence-guided resection with 5-ALA for malignant tumors, a significant difference was not observed between the optical properties of the glioblastoma regions with "strong" and "unobservable" fluorescence. However, the variation in hemoglobin contents caused by the use of *ex-vivo* measurement would affect these results. The μ_a values of glioblastoma tissue in the region with "strong" fluorescence and "unobservable" fluorescence were compared at 405 and 635 nm, and there was no significant difference. There were no significant differences between the μ_s' values of glioblastoma tissues in "strong" and "unobservable" fluorescence at 405 and 635 nm. The fluorescence signal strongly correlated with the tumor cell density. Although a higher cell density was found in "strong" and "unobservable" in fluorescence tissues, this is not reflected in the μ_a and the μ_s' spectra. In addition, from the result of the fluorescence Monte Carlo simulation, the ratio of the relative intensity of emission at the surface was almost identical. The δs at 405 nm in glioblastoma tissues with "strong" and "unobservable" fluorescence were about 0.28 ± 0.08 mm and 0.20 ± 0.05 mm, respectively. The small

amount of PpIX that is contained in the tissue within the depth of optical penetration more strongly affects the false negatives under the conditions that the tissue has low δ. Hence, it was considered that there was no correlation between fluorescence signals and the patient-averaged *ex-vivo* optical properties of the malignant glioma tissues. Thus, a false negative in using 5-ALA for detection of human glioblastoma does not result from the differences in optical properties of human brain glioblastoma tissues.

Disclosures

The authors have no financial interests and no other potential conflicts of interest to disclose in this article.

Acknowledgments

The Authors wish to express their appreciation to Dr. Takashi Yoneda for sample preparation. This development was supported by SENTAN, JST. This work was supported by JSPS KAKENHI (Grant No. 15K16322).

References

1. W. Stummer et al., "Intraoperative detection of malignant gliomas by 5-aminolevulinic acid-induced porphyrin fluorescence," *Neurosurgery* **42**(3), 518–526 (1998).
2. W. Stummer et al., "Fluorescence-guided surgery with 5-aminolevulinic acid for resection of malignant glioma: a randomised controlled multicentre phase III trial," *Lancet Oncol.* **7**(5), 392–401 (2006).
3. W. Stummer et al., "Extent of resection and survival in glioblastoma multiforme: identification of and adjustment for bias," *Neurosurgery* **62**(3), 564–576 (2008).
4. U. Pichlmeier et al., "Resection and survival in glioblastoma multiforme: an RTOG recursive partitioning analysis of ALA study patients," *Neuro-Oncology* **10**(6), 1025–1034 (2008).
5. W. Stummer et al., "Fluorescence-guided resection of glioblastoma multiforme by using 5-aminolevulinic acid-induced porphyrins: a prospective study in 52 consecutive patients," *J. Neurosurg.* **93**(6), 1003–1013 (2000).
6. D. W. Roberts et al., "Coregistered fluorescence-enhanced tumor resection of malignant glioma: relationships between δ-aminolevulinic acid-induced protoporphyrin IX fluorescence, magnetic resonance imaging enhancement, and neuropathological parameters. Clinical article," *J. Neurosurg.* **114**(3), 595–603 (2011).
7. K. Takahashi et al., "Enhanced expression of coproporphyrinogen oxidase in malignant brain tumors: CPOX expression and 5-ALA-induced fluorescence," *Neuro-Oncology* **13**(11), 1234–1243 (2011).
8. Y. Kajimoto and T. Kuroiwa, "Unsolved problems in 5-aminolevulinic acid based photodynamic diagnosis: quantification of fluorescence and molecular mechanism of porphyrin accumulation," *J. Jpn. Soc. Laser Surg. Med.* **32**(2), 143–148 (2011).
9. N. Honda et al., "Optical properties of tumor tissues grown on the chorioallantoic membrane of chicken eggs: tumor model to assay of tumor response to photodynamic therapy," *J. Biomed. Opt.* **20**(12), 125001 (2015).
10. L. Wang et al., "MCML-Monte Carlo modeling of light transport in multi-layered tissues," *Comput. Methods Programs Biomed.* **47**(2), 131–146 (1995).
11. V. V. Tuchin, "Optical properties of tissues with strong (multiple) scattering," Chapter 1 in *Tissue Optics: Light Scattering Methods and Instruments for Medical Diagnosis*, V. V. Tuchin, Ed., pp. 3–17, SPIE Press, Bellingham, Washington (2007).
12. B. Kemper et al., "Integral refractive index determination of living suspension cells by multifocus digital holographic phase contrast microscopy," *J. Biomed. Opt.* **12**(5), 054009 (2007).
13. "Scattering and absorption properties of diffusive media," Chapter 2 in *Light Propagation Through Biological Tissue and Other Diffusive Media*, F. Martelli et al., Eds., pp. 9–28, SPIE Press, Bellingham, Washington (2010).
14. S. L. Jacques, "Monte Carlo simulations of fluorescence in turbid media," Chapter 6 in *Handbook of Biomedical Fluorescence*, M. A. Mycek and B. W. Pogue, Eds., pp. 61–107, Marcel-Dekker, New York (2003).
15. G. I. Lozovaya et al., "Protoporphyrin IX as a possible ancient photosensitizer: spectral and photochemical studies," *Origins Life Evol. Biosphere* **20**, 321–330 (1990).
16. A. Johansson et al., "5-aminolevulinic acid-induced protoporphyrin IX levels in tissue of human malignant brain tumors," *Photochem. Photobiol.* **86**, 1373–1378 (2010).
17. L. O. Svaasand and R. Eixingsen, "Optical penetration in human intracranial tumors," *Photochem. Photobiol.* **41**, 73–76 (1985).
18. A. N. Yaroslavsky et al., "Optical properties of selected native and coagulated human brain tissues in vitro in the visible and near infrared spectral range," *Phys. Med. Biol.* **47**(12), 2059–2073 (2002).
19. S. C. Gebhart et al., "In vitro determination of normal and neoplastic human brain tissue optical properties using inverse adding-doubling," *Phys. Med. Biol.* **51**, 2011–2027 (2006).
20. A. Roggan et al., "The effect of preparation technique on the optical parameters of biological tissue," *Appl. Phys. B* **69**(5), 445–453 (1999).
21. A. Pitzschke et al., "Optical properties of rabbit brain in the red and near-infrared: changes observed under in vivo, postmortem, frozen, and formalin-fixated conditions," *J. Biomed. Opt.* **20**(2), 025006 (2015).
22. J. M. Brown and W. R. Wilson, "Exploiting tumor hypoxia in cancer treatment," *Nat. Rev. Cancer* **4**(6), 437–447 (2004).
23. R. J. Diaz et al., "Study of the biodistribution of fluorescein in glioma-infiltrated mouse brain and histopathological correlation of intraoperative findings in high-grade gliomas resected under fluorescein fluorescence guidance," *J. Neurosurg.* **122**(6), 1360–1369 (2015).
24. A. Bogaards et al., "Increased brain tumor resection using fluorescence image guidance in a preclinical model," *Lasers Surg. Med.* **35**(3), 181–190 (2004).
25. V. X. Yang et al., "A multispectral fluorescence imaging system: design and initial clinical tests in intra-operative photofrin-photodynamic therapy of brain tumors," *Lasers Surg. Med.* **32**(3), 224–232 (2003).
26. R. Splinter and B. A. Hooper, "Light-tissue interaction variables," Chapter 5 in *An Introduction to Biomedical Optics*, R. Splinter and B. A. Hooper, Eds., pp. 121–154, Taylor and Francis, London (2007).
27. S. L. Jacques and S. A. Prahl, "Limits of diffusion theory," Oregon Medical Laser Center, Providence St. Vincent Medical Center, 1998, http://omlc.org/classroom/ece532/class5/limits.html (20 October 2015).
28. D. Wirth et al., "Fluorescence depth estimation from wide-field optical imaging data for guiding brain tumor resection: a multi-inclusion phantom study," *Biomed. Opt. Express* **8**(8), 3656–3670 (2017).
29. P. A. Valdés et al., "Quantitative, spectrally-resolved intraoperative fluorescence imaging," *Sci. Rep.* **2**, 798 (2012).
30. P. A. Valdés et al., "qF-SSOP: real-time optical property corrected fluorescence imaging," *Biomed. Opt. Express* **8**(8), 3597–3605 (2017).
31. M. Sibai et al., "Quantitative spatial frequency fluorescence imaging in the sub-diffusive domain for image-guided glioma resection," *Biomed. Opt. Express* **6**(12), 4923–4933 (2015).
32. H. A. Leroy et al., "Fluorescence guided resection and glioblastoma in 2015: a review," *Lasers Surg. Med.* **47**(5), 441–451 (2015).
33. S. Eljamel, "5-ALA fluorescence image guided resection of glioblastoma multiforme: a meta-analysis of the literature," *Int. J. Mol. Sci.* **16**(5), 10443–10456 (2015).
34. J. Bravo et al., "Hyperspectral data processing improves PpIX contrast during fluorescence guided surgery of human brain tumors," *Sci. Rep.* **7**, 9455 (2017).
35. P. A. Valdés et al., "Combined fluorescence and reflectance spectroscopy for in vivo quantification of cancer biomarkers in low- and high-grade glioma surgery," *J. Biomed. Opt.* **16**(11), 116007 (2011).
36. W. Stummer et al., "5-Aminolevulinic acid-derived tumor fluorescence: the diagnostic accuracy of visible fluorescence qualities as corroborated by spectrometry and histology and postoperative imaging," *Neurosurgery* **74**(3), 310–320; discussion 319–320 (2014).
37. T. Ishikawa et al., "Key role of human ABC transporter ABCG2 in photodynamic therapy and photodynamic diagnosis," *Adv. Pharmacol. Sci.* **2010**, 587306 (2010).

Biographies for the authors are not available.